EUROFUSION WPMST1-CP(16) 15157

G Papp et al.

Runaway electron generation and mitigation on the European medium sized tokamaks ASDEX Upgrade and TCV

Preprint of Paper to be submitted for publication in
Proceedings of 26th IAEA Fusion Energy Conference

This work has been carried out within the framework of the EUROfusion Consortium and has received funding from the Euratom research and training programme 2014-2018 under grant agreement No 633053. The views and opinions expressed herein do not necessarily reflect those of the European Commission.

Runaway electron generation and mitigation on the European medium sized tokamaks ASDEX Upgrade and TCV

G. Papp[1], G. Pautasso[1], J. Decker[2], M. Gobbin[3], P.J. McCarthy[9], P. Blanchard[2], D. Carnevale[10], D. Choi[2], S. Coda[2], B. Duval[2], R. Dux[1], B. Erdős[4], B. Esposito[10], O. Ficker[5], R. Fischer[1], C. Fuchs[1], C. Galperti[2], L. Giannone[1], A. Gude[1], B. Labit[2], K. Lackner[1], T. Lunt[1], L. Marelli[3], P. Martin[3], A. Mlynek[1], E. Nardon[8], M. Maraschek[1], P. Marmillod[2], M. Nocente[6], Y. Peysson[8], P. Piovesan[3], V.V. Plyusnin[7], G.I. Pokol[4], P.Zs. Poloskei[4], S. Potzel[1], C. Reux[8], F. Saint-Laurent[8], O. Sauter[2], B. Sieglin[1], U. Sheikh[2], C. Sommariva[8], W. Suttrop[1], G. Tardini[1], M. Teschke[1], D. Testa[2], W. Treutterer[1], M. Valisa[3], ASDEX Upgrade Team[1], TCV Team[2] and the EUROfusion MST1 Team[*]

[1]Max-Planck-Institute for Plasma Physics, D-85748 Garching, Germany
[2]Swiss Plasma Centre, EPFL, CH-1015 Lausanne, Switzerland
[3]Consorzio RFX, corso Stati Uniti 4, 35127 Padova, Italy
[4]Institute of Nuclear Techniques, BME, Pf 91, H-1521 Budapest, Hungary
[5]Institute of Plasma Physics AS CR, Za Slovankou 3, 18200 Prague 8, Czech Republic
[6]Università di Milano-Bicocca, Piazza della Scienza 3, 20126, Milano, Italy
[7]Instituto de Plasmas e Fusão Nuclear, IST, Universidade de Lisboa, Portugal
[8]CEA, IRFM, F-13108 Saint Paul Lez Durance, France
[9]Department of Physics, University College Cork, Cork, Ireland
[10]ENEA sulla Fusione, C.R. Frascati, C.P. 65, 00044 Frascati, Roma, Italy
[*]See appendix of H. Meyer et.al. (OV/P-12) Proc. 26th IAEA Fusion Energy Conf. 2016, Kyoto, Japan

Corresponding Author: ppg@ipp.mpg.de

Abstract:
ASDEX Upgrade (AUG) and TCV have recently joined the international effort of better understanding runaway electron (RE) generation and dissipation, aiding the development of the future ITER disruption & runaway electron mitigation system. The AUG post-disruption RE beams can carry up to 400 kA of current and last up to 500 ms. Suppression of REs was achieved with 0.17 bar·l of argon or 0.7 bar·l of neon massive gas injection (MGI) into a fully formed beam using the in-vessel valves. A resonant magnetic perturbation configuration was developed that leads to up to a factor of 2 decrease in the RE current. TCV quiescent RE scenarios show RE generation at $E/E_c \gtrsim 15$. MGI induced disruptions can achieve a full conversion of Ohmic current into runaways and beam lengths of up to 650 ms. High-Z injections of argon & neon on TCV lead to enhanced RE dissipation, but not a full suppression. Elongated plasmas were found to not generate RE beams. Pre-disruption seed electrons have been found to survive the disruption on both tokamaks, indicating a partially confined core during the quench phase.

1 Introduction

Disruptions in tokamaks can lead to the generation of a relativistic runaway electron (RE) beam that may cause serious damage to the first wall. The avalanche effect increases the number of runaways exponentially, leading to runaway currents of several megaamperes in a large tokamak. The uncontrolled loss of such a high energy electron beam is intolerable and therefore the issue of how to avoid or mitigate an RE beam is of prime importance for ITER [1, 2]. The European medium sized tokamaks ASDEX Upgrade (AUG) [3] and TCV [4] have recently joined the international effort [5–16] of better understanding runaway electron dynamics, aiding the development of the future ITER disruption & runaway electron mitigation system. This paper reports on the first ever deliberately generated post-disruption runaway electron beams on these two tokamaks, and discusses the main characteristics of runaway generation & dissipation in the presence of high-Z materials such as neon or argon.

2 ASDEX Upgrade runaway scenario

The AUG RE scenario [17, 18] is based on a $B_T = 2.5$ T toroidal magnetic field, $I_p = 800$ kA plasma current, circular, inner wall limited, low central electron density ($\sim [2.5-3.6]\cdot 10^{19}$ m^{-3}), Ohmic, L-mode discharge with $2-2.5$ MW of Electron Cyclotron Resonance Heating (ECRH) applied for 100 ms just before the injection of $0.05-0.2$ bar·l ($[1.2-4.8]\cdot 10^{21}$ particles, about 14.5× the plasma inventory) of argon gas from a low field side in-vessel piezo valve (IVV) [19] with a volume of 100 cm^3. A peak density increase of $3-5\times$ is observed during the induced thermal quench and the subsequent RE beam phase. Spectroscopic analysis suggests that in the beam phase the density of singly-ionized argon is comparable to the free electron density [18]. The circular shape was chosen for better post-disruptive vertical stability, and the low density operation prevents the usage of Neutral Beam Injection (NBI) or longer ECRH for heating. Argon gas is injected with a pre-set trigger 1 s after the start of the discharge, at the end of the ramp-up.

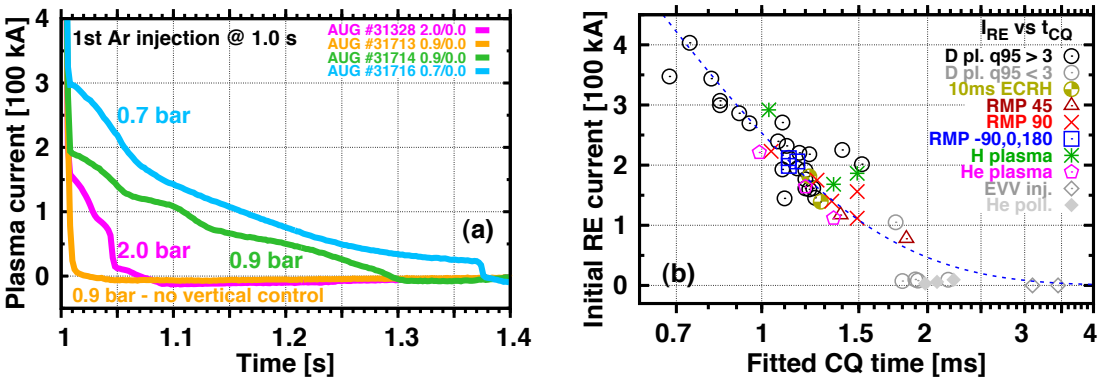

FIG. 1: (a) Runaway current evolution following various amounts of primary argon gas injections. (b) I_{RE} vs t_{CQ} fitted current quench time (note that the t_{CQ}-axis is logarithmic). The points follow a general trend, with a threshold for RE beam formation at $t_{CQ} \simeq 1.8$ ms.

The argon MGI produces a well reproducible disruption with a thermal quench time $t_{\mathrm{TQ}} < 1$ ms and leads to the generation of 100-400 kA of initial runaway electron current (examples are presented in Fig. 1a). After the first few ms following the CQ, the beams are in a controlled ramp-down. Discharges carried out in hydrogen plasmas lead to results comparable to deuterium, whereas in helium plasmas slightly lower RE current was achieved. Utilizing the control system it was possible to decrease or increase the RE plateau duration by about a factor of 2, up to the maximum beam duration of $t_{\mathrm{RE}} \gtrsim 500$ ms. Both directions are limited by constraints on the power supply and the control system. A clear correlation was found between the t_{CQ} current quench time (calculated by fitting $I_p(t) \sim I_{\mathrm{RE}}^0 + I' \exp\{-t/t_{\mathrm{CQ}}\}$ exponential decays on the plasma current evolution between the TQ and the plateau phase) and the initial runaway electron current (Fig. 1b), regardless of the type of RE experiment being carried out (indicated by different point types). This trend is qualitatively reproduced by 1D simulations using GO [20], which calculates self-consistent electric field dynamics, runaway generation and atomic physics processes. For quantitative comparisons modeling of the TQ/CQ RE losses is necessary in the future. The RE generation threshold is observed at the fitted current quench time of $t_{\mathrm{CQ}} < 1.8$ ms. Fast infrared cameras and a pair of visible & infrared spectrometers (forward and backward views) [21] are employed to diagnose the RE synchrotron radiation to gain further information about the position, structure and energy/pitch distribution of the RE beam [22].

Partial core survival

In some shots co- or counter current ECCD was applied before the TQ. Co-current ECCD lead to a $\sim$ 25% longer beam, whereas counter-current ECCD resulted in a $\sim$25% lower RE current and $\sim$ 30% shorter beam. These results indicate that ECRH introduces a fast particle seed which survives the thermal quench, which suggests that a complete ergodization of the plasma core does not happen during the TQ [23].

Time-frequency resolved mode number analysis of the magnetic pick-up coils [24] (shown in Fig. 2) indicates that a core localized, anharmonic $(m, n) = (1, 1)$ mode starts to develop before the MGI. Signatures of a (1,1) mode are found for several ms after the TQ in almost all RE beams, but only if a (1,1) mode was present before the disruption.

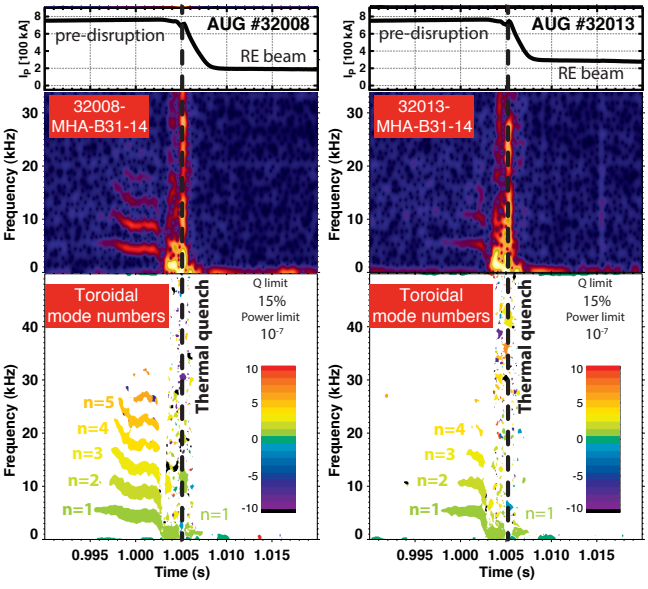

FIG. 2: Two examples for the formation of an anharmonic $(m, n) = (1, 1)$ mode before the MGI trigger at 1.0 s. Signatures of a $(1, 1)$ mode are visible briefly after the quench.

2.1 High-Z interaction

One of the main goal of these experiments is to better understand the interaction of REs with partially ionized high-Z materials. Discharges were carried out where a second MGI valve was triggered 70 ms after the first one, injecting various amounts of argon or neon from different geometrical locations. Suppression of REs was achieved with 0.17 bar·l of argon or 0.7 bar·l of neon using the IVVs (Fig. 3a). Argon injection from low or high field side IVV piezos lead to similar results. Following the injection of 0.32 bar·l from the high field side or 0.29 bar·l from the low field side the RE beam evolution was indistinguishable down to ∼50 kA, after which slight differences were observed. RE suppression was also possible using the ex-vessel electromagnetic valves [25], but more gas is required to do so. An injection of ∼0.25 bar·l of argon lead to only a partial suppression and 0.35 bar·l was necessary for full suppression, which is about a factor of 2 more than is required from the IVVs. JET did not succeed in RE suppression using secondary gas injection from ex-vessel valves [5], and while geometry was not considered to be the deciding factor, it was important to show the effect of the injection distance and location.

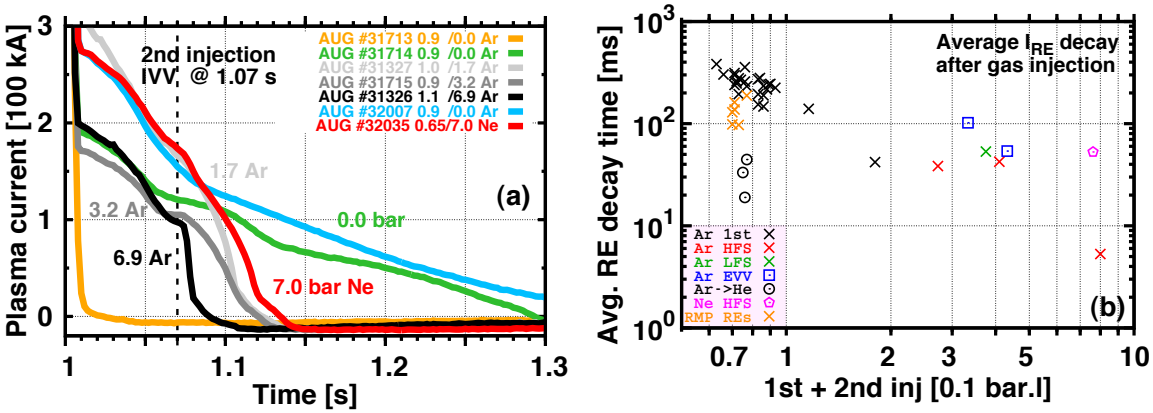

FIG. 3: Runaway current evolution following argon or neon secondary HFS IVV gas injections (at 1.07 sec) into an already formed beam. (b) Average RE decay time as a function of injected gas quantity. Crosses (×) represent IVV argon injection: black for only 1st injection, red/green for HFS/LFS 2nd injection, orange is for RMP shots. Circles (⊙) represent argon injection into He plasmas, while the pentagon (⬠) represents neon injection. Boxes (⊡) stand for EVV injection with representing a conservative estimate of the equivalent *injected* quantity.

Not all of the 2nd injection experiments could be carried out with the same baseline scenario. Therefore, for better comparison, a quantity normalized to the RE current, the average RE decay time τ_{RE} [s] $= I_{\mathrm{p\ t=1.07}}/\langle \mathrm{d}I/\mathrm{d}t\rangle_{\mathrm{RE}}$ is introduced and is plotted in figure 3b. Different injection / scenario types are represented with different point types and colors, as explained in the figure caption. Crosses (×) representing IVV argon injections seem to show a monotonic trend (note the log-log plot). However, injections between $0.2-0.5$ bar·l could also point to a saturation with the 0.7 bar·l 2nd injection being an outlier. The two-threshold theory of high-Z interaction [26] suggests a scaling of $\langle \mathrm{d}I/\mathrm{d}t\rangle_{\mathrm{RE}} \sim n_{\mathrm{Ar}}$. Note that the figure shows *injected* quantities, and corrections for different assimilation rates may be necessary. Further analysis and experiments are necessary to clarify this picture.

2.2 The effect of resonant magnetic perturbations (RMPs)

Multiple small and medium sized tokamaks reported results of RE mitigation using RMPs [27]. Test particle simulations suggest that an RMP-induced "stochastization" approach would probably not scale to ITER due to the size of the tokamak and the maximum current in the ELM perturbation coils (see Ref. [28] and references therein). The AUG RMP RE experiment considered two further possibilities: resonant mode amplification in the beam phase or influencing the disruption dynamics. Mode amplification was unsuccessful due to large edge q values ($q_{95} > 10$) in the RE beam phase.

The RMP system [29] was run in its most favorable configuration of $n = 1$, $I_{\rm RMP} = 1$ kA. As it takes several hundreds of milliseconds for the total perturbation field to build up (due to the surrounding conducting structures), which is comparable to the RE beam lifetime, the system was powered on 0.5 sec before the disruption was triggered. A relative phasing scan between the top and bottom coil set was carried out using the same ramp-up and gas injection scenario. $\Delta\phi = 0, +180°$ and $+270°$ had no effect on the RE beam. $\Delta\phi = 90°$ lead to a significant drop in $I_{\rm RE}$ and $t_{\rm RE}$, with $\Delta\phi = 45°$ having the strongest effect (see Fig. 4a,c). Figure 4b shows (normalized) calculated values of the $m = 4$ component of the perturbed magnetic field as a function of $\Delta\phi$ relative phasing for the pre-disruption (-■-) and post-disruption (-●-) equilibria. (Note that the *absolute* value of the perturbation is about $5 - 10\times$ higher in the pre-disruption phase.) Figure 4c shows the initial runaway plateau current $I_{\rm RE}(\Delta\phi)$ normalized to the mean value without perturbation. Strongest reduction ($\sim 35\%$ of unperturbed current) is observed for $\Delta\phi = 45°$ (coinciding with the strongest δB for pre-disruption), with significant reduction also at $\Delta\phi = 90°$ ($65 \pm 15\%$), which corresponds to maximum δB for post-disruption. The application of RMPs increased the current quench time by up to a factor of 2, and the beam currents decreased along the general trend (see Fig. 1b). This indicates that the perturbation has a significant effect on the disruption dynamics and RE beam formation.

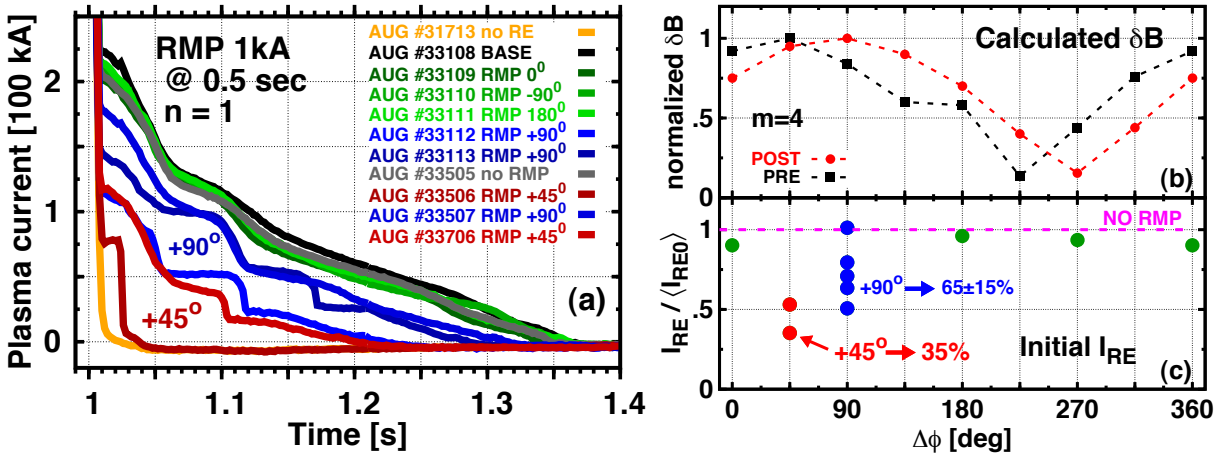

FIG. 4: (a) RE beams of the RMP phasing scan: $\Delta\phi = 90°$ and $\Delta\phi = 45°$ caused a significant drop in $I_{\rm RE}$ and $t_{\rm RE}$. (b) Calculated $\delta B(\Delta\phi)_{\rm m=4}$ values for pre- (-■-) and post-disruption (-●-) equilibria. (c) Initial RE current $I_{\rm RE}(\Delta\phi)$ normalized to the mean value without perturbation.

3 TCV RE experiments

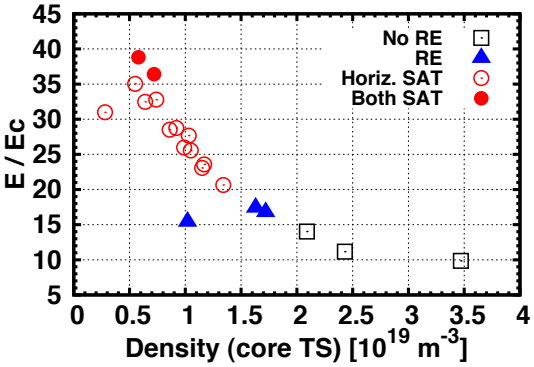

FIG. 5: HXR blind detector signals as a function of n_e (core TS) and E/E_c.

On TCV both quiescent and post-disruptive runaway scenarios were studied. The main diagnostic tool is two arrays of multi-chord hard X-ray (HXR) spectrometers, mounted on a top and an equatorial port[30]. For most RE discharges discussed in this paper some of the HXR photons are energetic enough to penetrate the collimator ($\epsilon_{\mathrm{HXR}} > 500$ keV), therefore the "blind" detector channels are used for RE detection. As most of the HXR radiation comes from forward-directed Bremsstrahlung [31], the horizontal camera is expected to pick up a stronger signal than the vertical one. In all cases the baseline scenario starts with a $B_{\mathrm{T}} = 1.43$ T, $I_{\mathrm{p}} = 200$ kA, $T_{e,0} = \mathcal{O}(1)$ keV, Ohmic, L-mode, inner wall limited, low density plasma.

For quiescent discharges line-averaged densities of $n_{\mathrm{e}} < 3{\cdot}10^{19}$ m^{-3} are used. Following the pre-fill the density is gradually dropped until REs appear, and in some cases the density is then ramped up again to study where the RE signal disappears. In the presence of sawteeth no hysteresis is observed, whereas without sawteeth a hysteresis is present, similar to e.g. DIII-D measurements [32]. This suggests that sawteeth with a period of $T_{\mathrm{ST}} \simeq 1$ms lead to an instantaneous loss of the REs, and consequently, the measured HXR signal is a signature of the RE generation rather than the accumulated RE population. Figure 5 shows the state of the HXR blind detector signals as a function of plasma density and electric field normalized to the critical field (E/E_c). No signal is present at $E/E_c < 15$, the horizontal camera goes into saturation at $E/E_c \simeq 20$, while both cameras are in saturation if $E/E_c > 35$. The observation threshold value around $E/E_c \simeq 15$ coincides with the findings of the ITPA joint experiment [13] and the current theoretical understanding of near-critical runaway scenarios [33].

A robust, well repeatable post-disruption RE scenario was achieved at unusually low pre-disruption line-averaged densities of $n_e < 2.5 \cdot 10^{18}$ m^{-3} using both argon and neon MGI at various pressures and injection quantities. While the quality of the MGI gas has an influence on the RE decay rate after the disruption, in both cases a seemingly full conversion of Ohmic into RE current was achieved (see Fig. 6a-b), as evidenced by the vanishingly low bulk electron temperature (< 20 eV) and current decay time – at zero applied loop voltage – much longer than the L/R time of the bulk. The RE beams start at the pre-disruption current (typically $I_p = 200$ kA) and last for several hundred ms with a record length of 650 ms. The full conversion is extremely sensitive to a pre-disruption density threshold, $n_e = 2.5 \cdot 10^{18}$ m^{-3} leads to a fast decaying beam with a lifetime of ~ 100 ms, while increasing the density higher suppresses RE generation completely. Further decreasing the density while under the threshold does not change the RE beam evolution significantly. The full conversion is attributed to a seed of preexisting "hot" electrons already generated in the plateau phase, as is evidenced by a well defined drop in the loop voltage (see Fig. 6c-d, at $t \simeq 0.35 - 0.4$ sec). This also suggests that similarly to AUG, part of the plasma core and the seed electrons survive the thermal quench.

One of the main goals of the TCV experiments was to utilize TCV's flexible plasma shape and position control to develop RE beam control methods [34] and to determine the direct and indirect effects of plasma shaping on RE generation and dissipation. The relative vertical position of the MGI valve with respect to the plasma was found to have a strong impact on impurity penetration into the plasma and, consequently, on the RE beam evolution. Injecting gas at the level of the plasma upper point ("tangential" injection) led to a higher post-MGI electron density and faster RE beam decay than shooting directly into the plasma ("radial" injection). Using the ohmic drive, the RE current can be ramped down significantly ($\sim 2\times$) faster than its natural evolution, or maintained for the entire duration of the remaining shot. An already formed RE beam can be moved up to 30 cm vertically. At the most favorable vertical position for control, a decaying RE beam can be kept under control down to a current of ~ 20 kA. During the RE beam phase, a series of sudden events can lead to partial loss of the RE current associated with bursts of HXR and visible emission. In some cases these events led to a complete loss of the RE beam. This is in clear contrast to the typical AUG beams which are inherently stable and show virtually no signals of bursts or loss events.

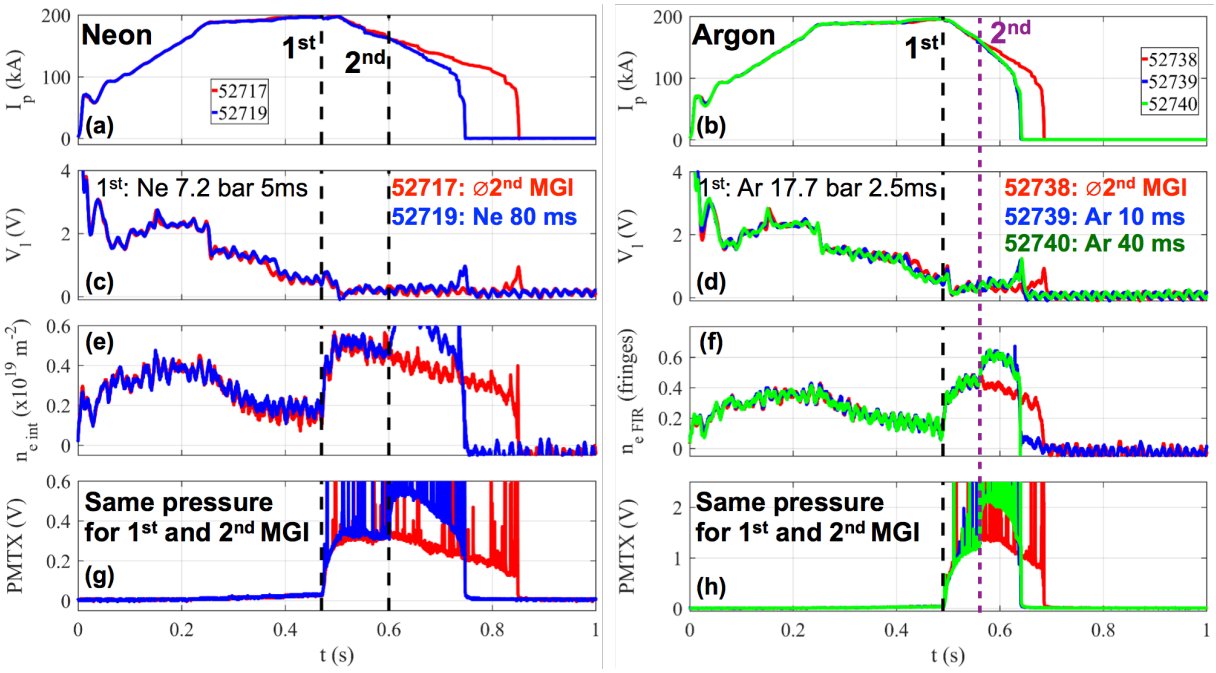

FIG. 6: Examples of RE beams and the effect of 2nd high-Z injection on TCV. Left: neon, right: argon 1st & 2nd injections. Evolution of plasma current (a-b), loop voltage (c-d), line-integrated density (e-f) and X-ray signals (g-h). Colors indicate the different 2nd injections.

In the plasma shaping studies the main challenge is getting the exact same plasma density before the disruption (given the sensitive density threshold). The scenario which was developed with an elongation of $\kappa = 1.4$ (while keeping the plasma top position fixed), lead to no post-disruptive RE beam formation. Higher elongations, while technically possible at TCV, were difficult to execute without changes to the density evolution. Changes of elongation in quiescent scenarios also changed the RE dynamics, but the shaping changes

sawtooth behaviour (which has an influence on REs) and therefore drawing conclusions requires more analysis.

Injection of high-Z materials into an already formed beam was also performed on TCV, and examples are shown in figure 6. As TCV is equipped with a singular ex-vessel electromagnetic valve, multiple injections can only be carried out with the same gas and pressure within the same shot. Both argon and neon injections lead to an increased RE dissipation, but not to the same extent as on AUG using the IVVs. Also, increasing the valve opening time during the 2nd injection lead to saturation. An example is shown in the argon case of figure 6 (right), where no significant difference is observable between 10 ms and 40 ms valve opening times at 17.7 bar of argon pressure.

4 Summary

Dedicated runaway electron experiments were carried out for the first time on both ASDEX Upgrade and TCV. Robust quiescent (TCV) and post-disruption (TCV & AUG) runaway scenarios were developed with a runaway current conversion of up to 50% on AUG and 100% on TCV. The beams are position controlled down to a current of 20 kA, posing little risk to the plasma facing components. Secondary MGI of argon or neon lead to an increased dissipation of RE beams. Using in-vessel valves a full suppression of the RE beam is possible on AUG. Results indicate a survival of the preexisting seed population during the TQ on both machines. Resonant magnetic perturbation was found to influence the TQ dynamics and decrease the RE current by $\sim 50\%$ on AUG. Elongated TCV plasmas were found not to generate post-disruptive RE beams. Further experiments, data analysis and detailed numerical modeling is planned in the future.

Acknowledgements The authors are grateful to J. Stober, S. Denk, M. Willensdorfer, V. Mertens, Ph. Schneider, S. Newton, T. Hayward, D. Coster and Ph. W. Lauber for fruitful discussions. This work has been carried out within the framework of the EUROfusion Consortium and has received funding from the Euratom research and training programme 2014-2018 under grant agreement No 633053. The views and opinions expressed herein do not necessarily reflect those of the European Commission.

References

[1] E. M. Hollmann et al. PoP, **22**:021802 (2015).
[2] M. Lehnen et al. JNM, **463**:39 (2015).
[3] A. Kallenbach et al. This conf., OV/2–1 (2016).
[4] S. Coda et al. This conf., OV/P–1 (2016).
[5] C. Reux et al. NF, **55** (9):093013 (2015).
[6] E. M. Hollmann et al. PoP, **22** (5):056108 (2015).
[7] K. Wongrach et al. PoP, **22** (10):102508 (2015).
[8] F. Saint-Laurent et al. In *ECA*, 35G O3.118 (2011).
[9] J. R. Martín-Solís et al. PRL, **105**:185002 (2010).
[10] R. J. Zhou et al. PoP, **21** (6):063302 (2014).
[11] Z. Y. Chen et al. PPCF, **55** (3):035007 (2013).
[12] M. Vlainic et al. JPP, **81**:475810506 (2015).
[13] R. S. Granetz et al. PoP, **21** (7):072506 (2014).
[14] V. Plyusnin et al. This conf., EX/P6–33 (2016).
[15] P. Martin et al. This conf., EX/P6–23 (2016).
[16] D. Carnevale et al. This conf., EX/P8–22 (2016).
[17] G. Pautasso et al. In *ECA*, 39E P1.134 (2015).
[18] G. Pautasso et al. PPCF, **submitted** (2016).
[19] G. Pautasso et al. NF, **55** (3):033015 (2015).
[20] G. Papp et al. NF, **53** (12):123017 (2013).
[21] B. Esposito et al. PPCF, **submitted** (2016).
[22] A. Stahl et al. PoP, **20** (9):093302 (2013).
[23] V. Izzo et al. NF, **51** (6):063032 (2011).
[24] L. Horváth et al. PPCF, **57** (12):125005 (2015).
[25] G. Pautasso et al. NF, **47** (8):900 (2007).
[26] P. Aleynikov et al. PRL, **114**:155001 (2015).
[27] M. Lehnen et al. PRL, **100**:255003 (2008).
[28] G. Papp et al. JPP, **81**:475810503 (2015).
[29] W. Suttrop et al. PRL, **106**:225004 (2011).
[30] S. Gnesin et al. RSI, **79** (10):10F504 (2008).
[31] O. Embréus et al. NJP, **18** (9):093023 (2016).
[32] C. Paz-Soldan et al. PoP, **21** (2):022514 (2014).
[33] A. Stahl et al. PRL, **114**:115002 (2015).
[34] B. Esposito et al. This conf., EX/P8–27 (2016).